

Effects of cation siting and spin–spin interactions on the electron paramagnetic resonance (EPR) of Cu^{2+} exchanged X Faujasite zeolite

Chrispin O. Kowenje, Barry R. Jones, David C. Doetschman *,
Szu-Wei Yang, Charles W. Kanyi

Department of Chemistry, Binghamton University, State University of New York, Binghamton, New York 13902-6000, USA

Received 24 July 2006; accepted 14 September 2006

Available online 19 September 2006

Abstract

Copper(II) exchanged Na X Faujasite zeolite was cation exchanged at levels from one Cu(II) in 30 unit cells (0.033 Cu(II)/UC) to 38 Cu(II) per unit cell (38 Cu/UC) and was examined by continuous wave and two-pulse and three-pulse electron paramagnetic resonance (EPR) at temperatures from 10 K to 300 K. In this work exchange of Cu^{2+} into X Faujasite zeolite is shown by EPR spectral and pulsed EPR relaxation measurements to begin into site I', where it lies coordinated to a hexagonal prism face with Si:Al ratios of predominantly 4:2 and 5:1. Spin–spin interactions influence EPR g -value averaging, spin–spin relaxation, and spin spectral diffusion in a manner highly dependent on Cu exchange. Spin–lattice relaxation is relatively independent of exchange. The marked increase observed in spin–spin relaxation and g -value averaging at 8 Cu/UC and an effective Cu–Cu distance of 1.2 nm can be understood in terms of filling sodalite cages with an average of 1 Cu^{2+} each.

© 2006 Elsevier B.V. All rights reserved.

Keywords: Zeolite; Faujasite; Electron paramagnetic resonance; Copper exchange; Spin–spin interactions; Cation sites

1. Introduction

Copper(II) exchanged zeolites are well-known aluminosilicate materials and useful as catalysts [1–6]. They have high catalytic activity for NO_x decomposition and for the selective reduction of certain hydrocarbons [7–9]. Zeolites have the advantage of physically trapping metal complexes in the pores and channels of the structure and not solely on external surfaces [1,2,10–14]. The present study is part of a study of transition metal ion exchanged NaX, for the purpose of developing a colorimetric sensor array whose elements are NaX exchanged with different cations. The hypothesis is that the differently exchanged NaX sensor elements would display recognizable responses to various adsorbed molecular gases capable of complexing to the

exchanged cations in the zeolite. A variety of spectroscopic methods, including EPR, were brought to bear on understanding the responses of the variously exchanged zeolites to a variety of adsorbed molecules capable of complexing the transition metal ion. This report is the outcome of the control EPR study of the uncomplexed Cu^{2+} exchanged NaX.

Faujasite zeolites have several cations sites [11,15] within their structure of sodalite cage units, tetrahedrally connected through sodalite hexagonal faces [16,17]. Hexagonal and subsequent geometrical designations refer to the interconnecting framework of metal atom tetrahedra, MO_4 (see Fig. 1). The sodalite cage has an approximately 0.66 nm internal diameter with six-ring windows of approximately 0.26 nm [11,18–20]. The sodalite interconnection creates a three dimensional structure with twelve-ring windows of approximately 0.74 nm in diameter about a “supercage” of approximately 1.18 nm diameter [11,18–20]. The sodalite interconnections are hexagonal prisms whose six-rings are

* Corresponding author. Tel.: +1 607 777 2298; fax: +1 607 777 4478.
E-mail address: ddoetsch@binghamton.edu (D.C. Doetschman).

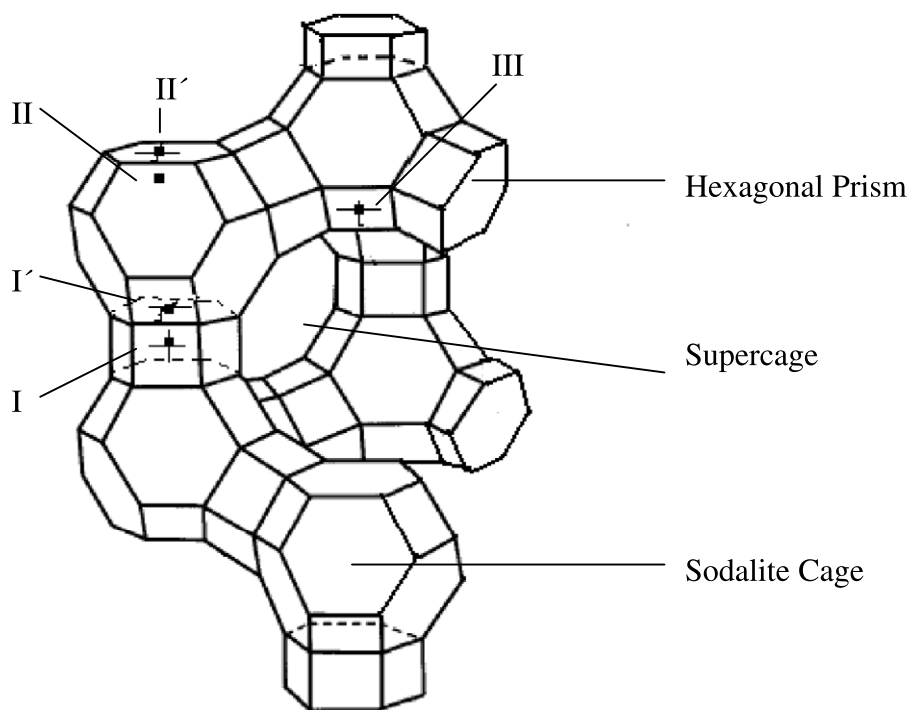


Fig. 1. Faujasite X cages and the cation exchange sites I–III.

those of the adjacent sodalite cages. Cation sites I and I' are at the center of the hexagonal prism or on the hexagonal prism axis, offset toward the sodalite cages, respectively. Likewise II, II' are axial sites slightly offset from or nearly at the center of the sodalite six-rings, opening into the supercage, respectively. Site III is on the supercage side of a sodalite four-ring.

Structural studies show Cu^{2+} to occupy primarily sites I', II, and III, [1,12,14,16,20] in which it is capable of compensating the charges from up to two framework Al. Cu^{2+} is also known to coordinate with anions, such as OH^- , whereby fewer Al charges are compensated [17,21,22]. Some of these studies suggest that a particular order exists for Cu^{2+} site preference with degree of exchange, beginning with site I' at low exchange, then site II, and finally to site III at high exchange [12,14].

EPR is an ideal tool for studying the sites occupied by the paramagnetic ion [8,13,19,23,24] and for learning about the relative locations of the Cu^{2+} from one another. The former application has the potential for distinguishing sites by means of the numbers of observed signals [2,4,14,16,23,25]. The anisotropic g -values and $^{63,65}\text{Cu}$ nuclear hyperfine coupling constants can shed light on the geometry of and charge distribution within the Cu^{2+} complex [2,4,14,23,25,26]. Fourier transform (FT) EPR techniques extend these capabilities for structural determination to the second coordination shell of Cu^{2+} [24]. Information concerning the relative locations of the Cu^{2+} from one another from EPR derives from the distance-dependent magnetic dipole interactions between paramagnetic copper ions [17,22,27,28].

The purpose of this study is thus to investigate with EPR the interrelated issues of Cu^{2+} siting in X Faujasite zeolite and the relative juxtaposition of Cu ions to one another, as functions of the degree of Cu^{2+} exchange. Considerable past work has been done employing EPR to investigate siting at relatively low exchange levels. Just a few EPR studies have been attempted to investigate relative Cu^{2+} siting by EPR at higher exchange levels [17,22,27–30] and considerable disagreement still exists among authors concerning the interpretation of the results. In this study, we examine systematically the continuous wave (CW) EPR spectra and the electron spin–spin and spin–lattice relaxation times with pulsed EPR of copper exchanged NaX zeolite, “CuX”, as a function of the degree of Cu exchange and temperature in order to understand these interrelated effects.

2. Experimental methods and theory

Zeolite NaX (Si/Al = 1.23, 2.0 μm particle size, Aldrich Chemical Co., used as received) was exchanged with aqueous solutions of $\text{Cu}(\text{NO}_3)_2 \cdot 2.5 \text{H}_2\text{O}$ (101.7% by EDTA complexation, J.T. Baker Chemical Co., as received). To weighted amounts of NaX in a flask were added amounts of 1.0 M $\text{Cu}(\text{NO}_3)_2$ sufficient to achieve the desired number of Cu ions per unit cell (Cu/UC) of zeolite. The slurry was brought to 20 mL of aqueous solution per gram of zeolite. The slurry was refluxed for 72 h at ca. 90 °C. After cooling and settling, the supernatant was decanted and the residue was centrifuged at 3500 rpm for 30 min. The centrifugate

was washed with deionized water (10 mL per gram of zeolite) and centrifuged. This procedure was repeated four times. Samples were Cu exchanged to levels from 0.033 Cu/UC to 38 Cu/UC.

Dehydrated CuX for the EPR studies was prepared from the exchanged, hydrated material in two steps. Firstly, the final centrifugate was air-dried in an oven at 60 °C for 48 h to remove non-coordinated water. Secondly, the air-dried CuX was dehydrated in a home-made, diffusion pump-driven, vacuum oven by raising the temperature 50 °C every 30 min to 450 °C at reduced pressures sufficiently high to avoid sample “dusting”. Upon reaching 450 °C the evacuation was continued for 4 h at vacuum approaching 10^{-8} torr. Samples were cooled to ambient temperature and were flame-sealed under vacuum in quartz EPR tubes.

The degree of exchange was gauged in the following way. The Cu/UC was determined from the drop in $\text{Cu}(\text{NO}_3)_2$ in solutions as a result of the exchange into the zeolite. The residual solutions, including washings, were analyzed for Cu content by flame atomic absorption (AA) (Perkin–Elmer Model 5000) spectrophotometry. (See the table of representative nominal and AA-based numbers of Cu per unit cell given in the [Supplementary Material](http://www.sciencedirect.com); <http://www.sciencedirect.com>).

CW EPR spectra were acquired with an ESP580 Bruker X-band (~ 9.5 GHz) spectrometer. Field sweeps 2000–3500 G were acquired at 1024 points with 100 kHz field modulation. Spectra were acquired at 10, 50, 70, 150 and 300 K employing an Oxford CF935 liquid helium cryostat and ITC temperature controller (to 1% of the desired temperature).

Pulsed EPR measurements of the decays of spin coherence and longitudinal magnetization were made on the same spectrometer using two- and three-pulse sequences. Measurements were made at the maximum in the echo intensity spectrum, found to be approximately at g_{\perp} . Microwave power was adjusted for $\pi/2$ and π pulses of 16 ns and 32 ns lengths, respectively. Inter-pulse times were optimized empirically to sample as much of the echo decay as possible, while avoiding cavity ring down. Decay times varied with the degree of Cu exchange. Typically 20 scans and 40 shots per point in the scan were averaged. The shot repetition time (SRT) was minimized, while avoiding microwave saturation, by incrementally increasing the SRT until the echo intensity no further increases. Measurements were all performed at 10 ± 0.1 K.

The CW EPR spectra were analyzed at low exchange levels by least squares fits of the g and A parameters in the Hamiltonian [27] in Eq. (1) to the spectra, where \underline{S} , \underline{I} ,

$$H = \beta_e \underline{B} \cdot \underline{g} \cdot \underline{S} + \underline{S} \cdot \underline{A} \cdot \underline{I} - g_n \beta_n \underline{B} \cdot \underline{I} \quad (1)$$

are the electron and nuclear spin angular momenta, respectively, and \underline{B} is the magnetic field. The \underline{g} and \underline{A} are pseudo-tensor interaction factors assumed to share principal axes and their principal values take on the symmetry, $g_{\parallel} = g_{zz}$, $g_{\perp} = g_{xx} = g_{yy}$ and $A_{\parallel} = A_{zz}$, $A_{\perp} = A_{xx} = A_{yy}$. The Cu d^9

system has $S = 1/2$ and the two Cu isotopes have $I = 3/2$. β_e and β_n are the electron and nuclear Bohr’s magneton, respectively.

At high Cu exchange levels the major features of the EPR spectra were found to be adequately described by Eq. (2) with symmetry $g_{\text{iso}} = g_{xx} = g_{yy} = g_{zz}$ and $A_{\text{iso}} = A_{xx} = A_{yy} = A_{zz}$. The g_{iso} values were compared with theoretical g_{av} values, calculated as in Eq. (2) for a dynamical process that would present the fast motion limit average

$$g_{\text{av}} = (1/3)(2g_{\perp} + g_{\parallel}) \quad (2)$$

environment of the anisotropic environments at low Cu exchange levels [29,31,32].

It is well-known that the presence of nuclear magnetic moments, coupled to the field-quantized electron spin through off diagonal interactions, are capable of modulating the electron spin echo decays. Modulations of this kind have been observed for the framework ^{27}Al nuclear spin coupling to the electron spin of the Cu^{2+} in Cu exchanged Faujasite. In order to determine the echo decay alone, the modulation must be factored out of the modulated decay. In a system where the modulations of a single nucleus of effectively $I = 1/2$ in a particular orientation in the magnetic field predominates, an experimental modulated echo intensity decay takes the form [33] given in Eq. (3), a situation that is found

$$I_{\text{echo}} = Ae^{-bt} [1 - C \sin^2(\omega_{\text{ab}}\tau/2) \sin^2(\omega_{\text{cd}}\tau/2)] \quad (3)$$

effectively to apply to the modulated decays in this work. The time τ is the pulse interval and the other quantities are variable parameters in the fitting process, including the observed decay rate b . (The quantities ω_{ab} and ω_{cd} correspond to the nuclear magnetic resonance angular frequencies of the nucleus in the upper and lower electron spin states, respectively.)

In order to determine the spin–spin relaxation rate of the Cu^{2+} spins in the samples, the effects of instantaneous diffusion [34–39] were subtracted from the observed two-pulse echo decay rates according to Eq. (4). Here b is the observed decay rate,

$$b = b_0 + b_{\text{ID}}[\sin^2(\theta/2)] \quad (4)$$

b_0 and b_{ID} are the true spin–spin relaxation rate and the instantaneous decay rate constant, respectively. The turning angle θ is the tip angle of the magnetization induced by the microwave pulse, such as $\pi/2$ or π for the pulses in a $\pi/2$ – π pulse sequence.

3. Experimental results

The EPR spectrum of 1 Cu/UC CuX at room temperature is shown in Fig. 2.

Two Cu(II) spectra can be resolved having $g_{\parallel} \approx 2.40$ and $A_{\parallel}/g_e\beta_e \approx 130$ G and $g_{\perp} \approx 2.35$ and $A_{\perp}/g_e\beta_e \approx 150$ G. The spectrum is broad and essentially unchanged, except for intensity, from 10 K to 300 K (See [Supplementary Material](http://www.sciencedirect.com); <http://www.sciencedirect.com>).

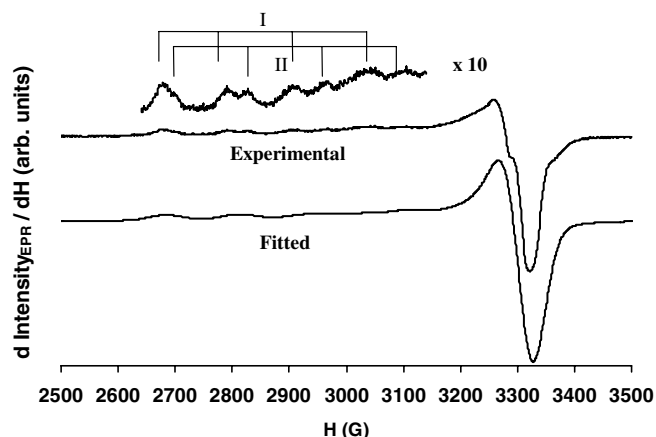


Fig. 2. Experimental (top) and least squares fitted (bottom) EPR spectra of 1 Cu/UC CuX at room temperature. The intensity of the parallel region of the experimental spectrum has been expanded to show the hyperfine lines of the Cu^{2+} species I and II. The least squares spectrum is a sum of the best fit spectra of Cu^{2+} species I and II.

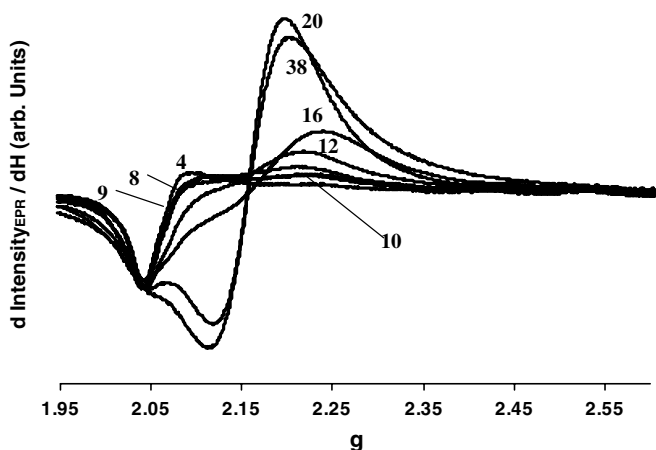


Fig. 3. The EPR spectra of dehydrated CuX at various degrees of exchange at room temperature, as indicated by the numbers in units of Cu/UC.

Fig. 3 gives the room temperature EPR spectra of CuX as a function of the degree of Cu exchange. The spectra have been transformed to a g scale with the Bruker spectrometer software. The spectra show the parallel features to be progressively more spread out and less pronounced with increasing Cu^{2+} exchange. Concomitantly, there appears at $g_{\text{iso}} \approx 2.16$ a signal progressively increasing in intensity with increasing exchange. However, at 20 Cu/UC, the signal associated with low concentration at $g_{\perp} \approx 2.06$ is still present but less pronounced. At 38 Cu/UC the only resolvable feature is the $g_{\text{iso}} \approx 2.16$ signal. A spectrum of a sample at 38 Cu/UC exhibiting predominantly the $g_{\text{iso}} \approx 2.16$ signal is largely unchanged, except for intensity, from 10 K to 300 K. However, a subtle narrowing of the averaged feature can be seen to occur progressively with increasing temperature. (See Supplementary Material; <http://www.sciencedirect.com>).

Fig. 4 shows the decay of the two-pulse ($\pi/2-\pi$) time-integrated echo signal for Cu at two exchange levels. Both

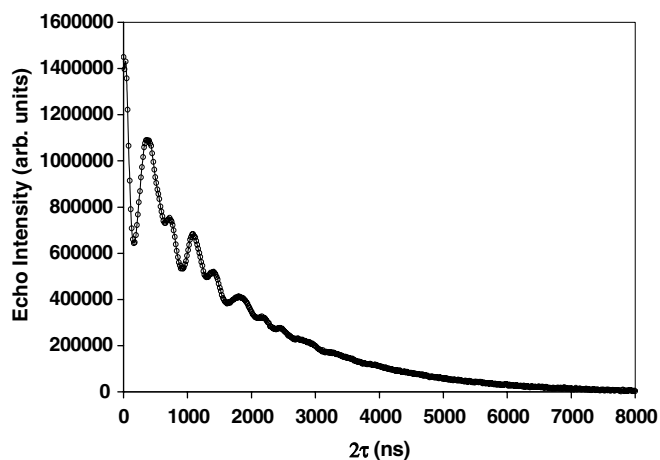
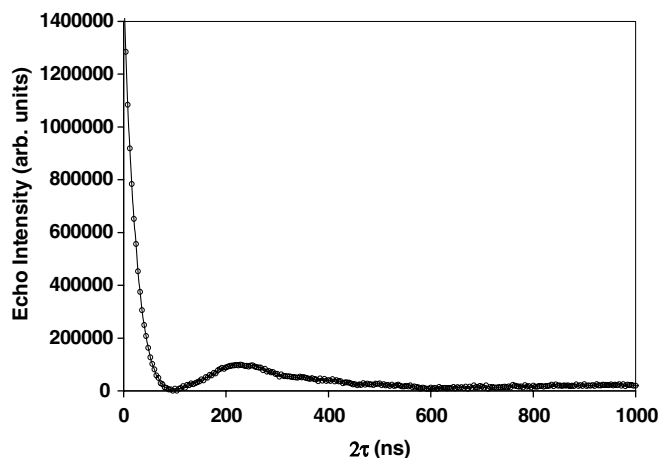


Fig. 4. Two-pulse echo decays of CuX, exchanged at 0.2 Cu/UC (top) and 8 Cu/UC (bottom). Echo intensity is plotted against the time $b = 2\tau$, the spin dephasing time of which T_2 is a measure, where τ is the time between microwave pulses.

appear as approximately exponential decays with modulations superimposed over them. The modulations superimposed on the decays are due to the hyperfine interactions of the copper electron spin with neighboring Al nuclei [27,28]. This figure highlights the increase in the coherence decay rate with increasing Cu exchange level. The modulations are more pronounced at low Cu exchange than at high exchange. Two-pulse echo decays were recorded on samples from 1 Cu/UC to 10 Cu/UC at 1 Cu/UC exchange level increments, as well as at 0.033, 0.1, and 0.2 Cu/UC. The time constants of these decays can be seen in Table 1, which also reports the analysis of the measured data to be discussed in the next section.

Fig. 5 shows a typical three-pulse ($\pi-\pi/2-\pi$) “inversion recovery,” where the measured time-integrated echo intensity is shown versus time elapsed between the first, “inversion” pulse and the $\pi/2-\pi$ probe part of the sequence. The measured curves have two regimes, a slowly recovering part over several hundred microseconds (top) and a quickly recovering part over several microseconds (bottom), not resolvable on the scale of the slowly recovering regime. The slowly recovering regime, which is not highly depen-

Table 1

Two-pulse echo decay times (T_M) and rates ($1/T_M$) and the spin–spin relaxation times T_2 derived from the echo decays at 10 K at various degrees of Cu^{2+} exchange into the zeolite

Copper exchange (Cu/UC)	EPR 2-pulse echo decay parameters		
	T_M (ns)	$1/T_M$ (MHz)	T_2 (ns)
0.033	3710 (40)	0.270 (.003)	3710 (40)
0.1	1210 (70)	0.826 (.046)	1210 (70)
0.2	1920 (40)	0.591 (.015)	2660 (6)
1	820 (520)	1.22 (0.77)	2100 (1300)
2	285 (12)	3.51 (0.15)	285 (12)
3	187 (45)	5.35 (1.29)	187 (45)
4	150 (24)	6.67 (1.05)	150 (24)
5	136 (15)	7.35 (0.81)	136 (15)
6	98.0 (8.7)	10.2 (0.9)	98.0 (8.7)
7	119 (3)	8.40 (0.19)	119 (3)
8	66.2 (2.6)	15.1 (0.6)	66.2 (2.6)
9	54.9 (1.8)	18.2 (0.6)	54.9 (1.8)
10	47.6 (2.0)	21.0 (0.9)	47.6 (2.0)

Bracketed quantities are the associated standard deviations.

Table 2

The spectral diffusion times (T_{SD}) and rates ($1/T_{SD}$) and the spin–lattice relaxation times (T_1) and rates ($1/T_1$) derived from the three-pulse inversion recoveries at 10 K at various degrees of Cu^{2+} exchange into the zeolite

Copper exchange (Cu/UC)	EPR three-pulse inversion recovery parameters			
	T_{SD} (ns)	$1/T_{SD}$ (MHz)	T_1 (μs)	$1/T_1$ (kHz)
0.033	4390 (500)	0.228 (0.026)	171 (7)	5.85 (0.24)
0.1	2730 (80)	0.366 (0.011)	106 (2)	9.43 (0.18)
0.2	2400 (200)	0.417 (0.035)	169 (8)	5.92 (0.28)
1	2280 (100)	0.439 (0.019)	127 (7)	7.87 (0.43)
2	2440 (90)	0.409 (0.015)	160 (2)	6.25 (0.08)
3	2100 (200)	0.465 (0.045)	63 (7)	15.9 (1.8)
4	2240 (60)	0.446 (0.012)	100 (10)	10.1 (1.0)
5	1300 (50)	0.769 (0.030)	106 (5)	9.44 (0.44)
6	1770 (60)	0.565 (0.019)	98 (5)	10.2 (0.5)
7	940 (30)	1.06 (0.03)	100 (5)	10.0 (0.5)
8	–	–	116 (4)	8.62 (0.30)

Bracketed quantities are the associated standard deviations.

4. Analysis

The experimental EPR spectra of CuX at 1 Cu/UC in Fig. 2 and at 38 Cu/UC in Fig. 3 were fitted by the spin Hamiltonian parameters by adjustment of the g and A pseudo-tensor principle values and Gaussian linewidth factors with the Bruker WINEPR Simfonia software version 1.2, 1995. The parameters were varied until least-squares best-fit agreement between the calculated and experimental spectral intensities was obtained. The existence of two spectra in the spectrum of 1 Cu/UC CuX in Fig. 2 was handled by fitting a linear combination of the intensities of two computed spectra to the experimental spectrum. This was accomplished with the additional variation of the intensity ratio of the two spectra. The linewidth and spin Hamiltonian parameter results are given in Table 3. The best fit at 1 Cu/UC also gave an intensity ratio of spectrum I to spectrum II of $1.28 \pm 0.03:1$. As a further measure of the temperature independence of the low exchange CuX spectra, these spectra at various temperatures were similarly fitted (See Supplementary Material; <http://www.sciencedirect.com>).

In order to test the hypothesis that the observed 38 Cu/UC spectrum is an average of the anisotropic spectra observed at 1 Cu/UC, Eq. (2) was employed to calculate $g_{av} = 2.156 \pm 0.001$ for species I and $g_{av} = 2.159 \pm 0.004$ for species II.

The peak to trough intensity of the $g_{iso} = 2.16$ EPR peak or feature, normalized to the total degree of Cu exchange, is presented in Fig. 6 as a function of Cu exchange in units of Cu–Cu distance. It is labeled “Int. of Avg. EPR Peak” standing for intensity of the averaged EPR peak, because, as will be discussed in the discussion section, it will be assigned to a dynamical average of the low concentration spectrum.

The two-pulse integrated echo intensity decays, such as the examples in Fig. 4, were least squares fit by Eq. (3) in order to determine the decay constants b . The other

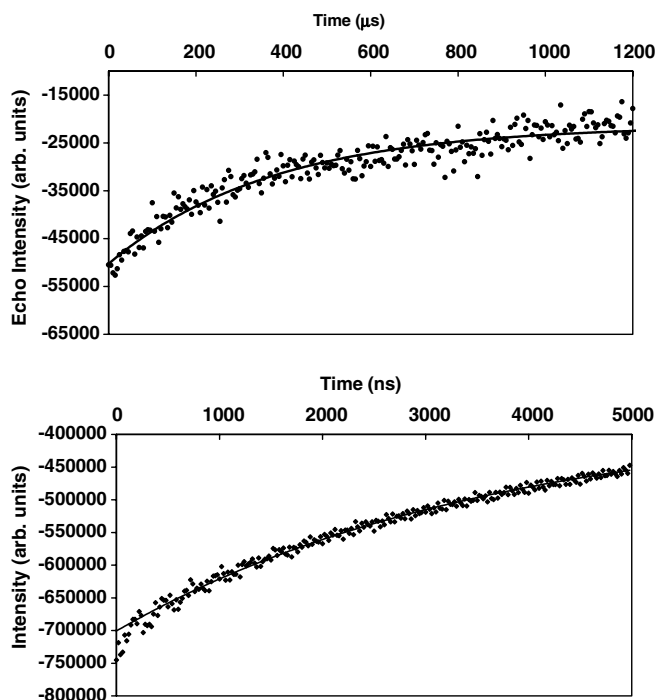


Fig. 5. Three-pulse inversion recovery of the 0.033 Cu/UC sample. The experiment was broken into two time regimes. The top plot shows the recovery up to 1200 μs and was fitted (solid line) to obtain T_1 . The bottom plot shows the early part of the recovery up to 5000 ns and was fitted (solid line) to obtain T_{SD} .

dependent on the degree of Cu exchange, was recorded on samples from 1 Cu/UC to 8 Cu/UC at 1 Cu/UC exchange level increments, as well as at 0.033, 0.1, and 0.2 Cu/UC. The quickly recovering regime, which is very dependent on the degree of Cu exchange, was measured over the same range of Cu exchange, except that the fast recovery was not measurable in the 8 Cu/UC sample. The time constants of these recoveries can be seen in Table 2.

Table 3
Spin Hamiltonian and linewidth parameters, L , for CuX at 1 Cu/UC and at 38 Cu/UC at room temperature

CuX exchange	g_{\parallel}	g_{\perp}	$\beta A_{\parallel}/h$ (G)	$\beta A_{\perp}/h$ (G)	L_{\parallel} (G)	L_{\perp} (G)
38 Cu/UC	2.159 (0.008)		24 (3.02)		115 (5.2)	
1 Cu/UC species I	2.363 (0.001)	2.051 (0.001)	127.0 (3.8)	5.0 (0.1)	55.0 (2.1)	45.5 (2.0)
1 Cu/UC species II	2.337 (0.002)	2.071 (0.006)	148.3 (4.8)	5.0 (0.1)	60.0 (3.0)	45.0 (2.5)

Bracketed quantities are the associated standard deviations. The values at 38 Cu/UC are isotropic and one value is given for both of the anisotropic parameters. The values for the species I and II both observed at 1 Cu/UC are given separately. The ratio of the two species was also analyzed and is given in the text.

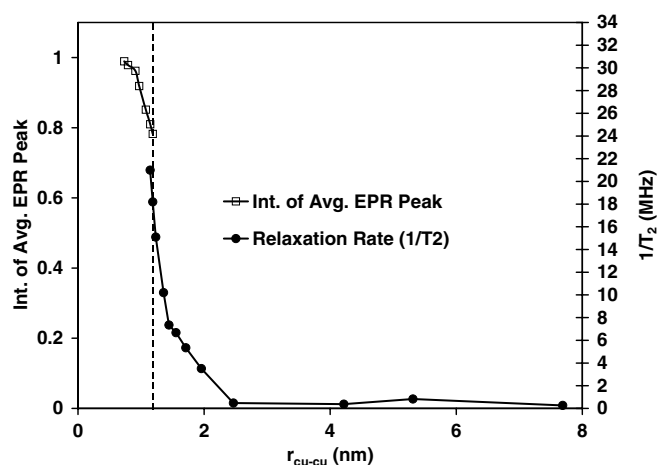


Fig. 6. Normalized peak-to-trough intensities of the isotropic, averaged, EPR peak (Int. of Avg. EPR Peak) observed in the CW EPR and the spin relaxation rates $1/T_2$, given as a function of the degree of Cu exchange. See Eq. (3) and accompanying discussion for the definition of the abscissa in terms of average Cu–Cu separation.

parameters in Eq. (3) are not of interest in this work and are not reported. However, we note that the ω_{ab} and ω_{cd} were reasonable in view of detailed echo modulation analyses [21,24]. An example of a fit to the echo decay in the case of the 6 Cu/UC CuX sample is shown in Fig. 7. The

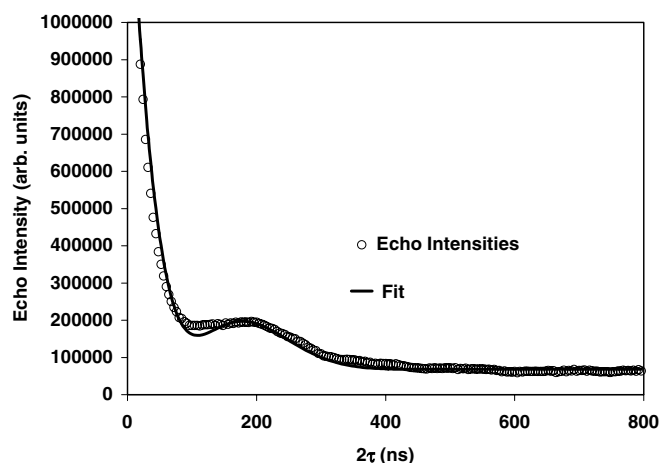


Fig. 7. Two-pulse echo decay of 6 Cu/UC CuX and the least squares fit to it with Eq. (3). Echo intensity is plotted against the time $b = 2\tau$, the spin dephasing time of which T_2 is a measure, where τ is the time between microwave pulses.

observed decay times T_M and decay rates $b = 1/T_M$ are presented in Table 1.

All of the samples were examined for the effects of instantaneous diffusion by plotting the observed decay rate b versus the $\sin^2(\theta/2)$ function of the magnetization turning angle θ , according to Eq. (4). Instantaneous diffusion was observed only in the 1 Cu/5 UC and 1 Cu/UC samples, a limited region of observation of instantaneous diffusion that has also been reported by others [35]. An example of the analysis of such a plot is given in the Supplementary Material; <http://www.sciencedirect.com>. The decay times $1/b = T_2$, checked and corrected in these two cases for instantaneous diffusion, are also presented in Table 1 and are plotted as a function of a measure of Cu–Cu distance in Fig. 6. No dependence on turning angle θ was observed for the other concentrations and thus the T_M and T_2 entries are identical at these other concentrations.

The three-pulse echo recovery curves, due to their nature, were acquired both at short times in the rapid recovery limit and at long times in the slow recovery limit.

In the homogeneously broadened EPR lines of CuX samples the Cu^{2+} electron spins have resonance frequencies spanning nearly 1000 G, whereas the π “inversion” pulse “burns” an inverted “hole” of the order of only 5 G. Likewise the $\pi/2$ – π probe pulse sequence also only probes a narrow portion of the spectrum.

The recovery will thus be governed by two, non-energy-conserving types of processes [35–37]. In one process, pairs of unlike spins exchange magnetization with one another, spreading the inversion outward into parts of the EPR line to the sides of the burned inversion hole and diminishing the inversion at the “hole”. Such processes are spectral diffusion processes and are known to have rates comparable with $1/T_2$, the spin–spin relaxation process in which like spins exchange magnetization. The second type of process is the spin–lattice relaxation process in which a spin flip exchanges energy with the zeolite crystal lattice at a rate $1/T_1$.

Thus, the three-pulse echo recovery data were analyzed by least squares fitting the data with exponential recovery curves. The fast recovery times, that will be seen to be comparable with T_2 and should be associated with spectral diffusion, are called T_{SD} and are tabulated in Table 2 along with the corresponding spectral diffusion rates, $1/T_{SD}$. Likewise the slow recovery time constants, associated with spin–lattice relaxation and known as T_1 , are tabulated in Table 2 along with the corresponding spin–lattice relaxation rates $1/T_1$.

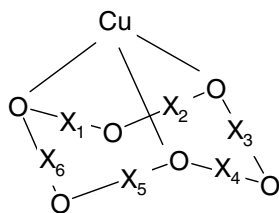


Fig. 8. Model of Cu^{2+} coordinated to hexagonal ring site I' of the zeolite framework. Coordination to three of the hexagonal ring oxygens is shown. X_1 – X_6 are the six framework metal sites occupied either by Si or Al.

In view of the importance of the Al ion distribution found in the FTEPR studies [21,24], we performed a statistical analysis to derive the probabilities of the various Si–Al distributions around a Cu^{2+} ion trigonally coordinated to the zeolite at site I'. Fig. 8 shows a Cu ion coordinated to three oxygen atoms in the six-ring of an X Faujasite hexagonal prism, site I'.

The Si:Al ratio of the starting X Faujasite was 1.23, making the Si and Al occupation probabilities, 0.55 and 0.45, respectively. For a simple, hypothetical example of our approach, consider a hypothetical site in which there are only two framework metal sites which may be occupied by Si or Al. Then the relative probability of both sites being occupied by Si would be 0.55^2 , the relative probability of occupation by one Si and one Al would be $2(0.55)(0.45)$, and the probability of both sites being occupied by Al would be 0.45^2 . The sum of these relative probabilities, which would also be the normalizing factor to obtain actual probabilities, would be $0.55^2 + 2(0.55)(0.45) + 0.45^2$. For the present case where there are six sites for the framework metal, the relative probabilities are given in the first column of Table 4.

However, a widely recognized restriction in the composition of an aluminosilicate material is that no two Al atoms occupy adjacent sites in order to avoid local concentration of charge [40]. This will change the relative probability distribution as a result of not all of the Si–Al distributions being permissible. We subtracted by inspection the number of forbidden arrangements from the coefficients of the relative probabilities, as shown in the second column and as evaluated in the third column of Table 4. In the last column of Table 4, we present the absolute probabilities based on the relative probabilities corrected for for-

bidden distributions. With the exception of two distributions with less the 10% probability, the ratio of the two most likely Si:Al compositions (4:2 and 5:1) is 1.23:1.

5. Discussion

The existence of two Cu^{2+} EPR spectra at low degrees of exchange has been explained in several different ways. Some authors associate the two spectra with Cu^{2+} at the sites I' and II of the zeolite framework [8,25,29] (see Fig. 1). Pierloot et al. [14] however, have noted that in examining a number of different zeolite types the number of Cu^{2+} EPR spectra observed does not match the number of sites available and similar observations have been reported by other authors [19,41]. Other authors associate the two species observable at low Cu exchange levels with different Al distributions at a single Cu^{2+} site [14,21,25]. Structural studies indicate that there is a preference for Cu^{2+} occupation of site I' at low exchange [9,12,42]. This preference is not consistent with a site I':II occupation ratio as low as 1.28:1, the ratio observed for the two Cu^{2+} spectra. Finally, the calculated ratio of 1.23:1 of the 4:2 Si:Al distribution to the 5:1 distribution in the site I' hexagonal ring is remarkably close to the observed ratio of 1.28:1 for the two observed Cu^{2+} EPR spectra. Thus our work provides further evidence that the two observed Cu^{2+} EPR spectra at low Cu exchange are from the predominantly site I' Cu^{2+} occupancy, which has mainly two Si:Al distributions in the site I' hexagonal ring. We note also that the site intensity ratio is not in as good agreement with the Cu isotope ratio and the *A* value ratio does not agree with the ratio of the magnetic moments of the Cu isotopes. Thus we also rule out the assignment to the two Cu isotopes.

This conclusion raises one new unanswered question about the nature of the overall charge compensation in the 5:1 Si:Al distribution, where the Cu^{2+} charge over-compensates the single negative charge on the hexagonal ring. The 4:2 ratio hexagonal rings are perfectly compensated by a Cu^{2+} .

It is well-known that magnetic dipole interactions between electron spins, which vary with inter-spin distance, *r*, as r^{-3} , lead to EPR line broadening phenomena [27,32]. Spins $S = 1/2$ generally become susceptible in the neigh-

Table 4

Statistical analysis of the Si and Al distributions around a Cu^{2+} coordinated at the hexagonal face site I'

Si:Al	Relative probability	Corrected relative probability	Evaluated corrected relative probability	Absolute probability
0:6	$1(0.45)^6$	$(1-1)(0.45)^6$	0	0
1:5	$6(0.55)(0.45)^5$	$(6-6)(0.55)(0.45)^5$	0	0
2:4	$15(0.55)^2(0.45)^4$	$(15-15)(0.55)^2(0.45)^4$	0	0
3:3	$20(0.55)^3(0.45)^3$	$(20-18)(0.55)^3(0.45)^3$	0.03032	0.08407
4:2	$15(0.55)^4(0.45)^2$	$(15-6)(0.55)^4(0.45)^2$	0.16677	0.46240
5:1	$6(0.55)^5(0.45)$	$(6-0)(0.55)^5(0.45)$	0.135887	0.37678
6:0	$1(0.55)^6$	$(1-0)(0.55)^6$	0.027681	0.07675

For each Si:Al ratio the relative probability calculation is shown in the first column, the second and third columns show the probabilities corrected for forbidden distributions and the fourth column shows the probabilities normalized to a total probability of one.

borhood of $r \approx 0.8$ nm [43] and this phenomenon is recognized as a difficulty in determining Cu^{2+} g values at high Cu^{2+} concentrations [31]. This work confirms the conclusion of other workers [21,28,44–46] that the rise of the EPR signal at $g_{\text{iso}} = 2.16$ with increasing Cu exchange, seen in Fig. 3 and plotted in Fig. 6, results from dynamic spin–spin interactions of proximate Cu^{2+} . The excellent agreement between the average g values calculated from the two Cu^{2+} spectra at low concentration, $g_{\text{av}} = 2.156 \pm 0.001$ and $g_{\text{av}} = 2.159 \pm 0.004$ for the species I and II and the observed value of $g_{\text{iso}} = 2.159 \pm 0.008$ is strong confirmation that dynamical averaging is occurring. The observation that the dynamically averaged spectrum in a 38 Cu/UC sample remains unchanged down to 10 K suggests a rapid process with a rate in excess of $\sim 2 \times 10^9 \text{ s}^{-1}$ at 300 K. The well-known ion site dependence on concentration [17,19,20,25] does not appear to provide a sufficient explanation of the observations in this study.

With rates as high as estimated from the averaging of high Cu exchange samples at 10 K, it is natural to inquire about the relation of the spin–spin dynamical averaging processes to spin–spin and spin–lattice relaxation and spin spectral diffusion processes. The data in Tables 2 and 3 confirm that both spin–spin relaxation and spectral diffusion processes are strongly dependent on the degree of Cu exchange, but spin–lattice relaxation has little dependence. This is not surprising in that both of the highly dependent processes have a contribution from the mutual spin–spin flip-flops that could also serve to average the EPR line at sufficiently high rates.

In order to demonstrate more effectively that the highly Cu exchange dependent relaxation process is probably the same process that averages the EPR line, we have plotted in Fig. 6 both the growth in intensity of the averaged EPR line and the spin–spin relaxation rate $1/T_2$ versus the degree of Cu exchange in units of Cu–Cu distance r ,

$$r = [N_{\text{Cu}}/V]^{-1/3} \quad (5)$$

where N_{Cu}/V is the number of Cu^{2+} per unit volume in the sample. It is remarkable that two scales can be chosen that achieve a respectable continuity between these two quantities and that the behavior of these two quantities points to a Cu–Cu distance, $r \approx 1.2$ nm at which spin–spin relaxation rates and the averaging of the EPR line are changing dramatically with the degree of Cu exchange. This corresponds to an exchange of about 8 Cu/UC.

One may legitimately inquire why the $1/T_2$ rates in Table 2, which we attribute to the spin–spin relaxation rates are not in agreement with the width of spin averaged feature in Fig. 3. The present study does not make it altogether clear why this is but one may speculate that either the low $1/T_2$ rates are not sufficiently fast to have reached the extreme narrowing regime or their may be residual heterogeneous broadening in the EPR line from different Cu sites and different environments around the Cu sites.

Finally consider the significance of 8 Cu/UC exchange in terms of the occupancy of sites versus degree of exchange. Assume, as confirmed still more conclusively by this work, that with increasing exchange, sites I' simply fill up until the onset of the filling of sites II. There are eight (8) sodalite cages per unit cell and each sodalite cage has four sites I' or a total of 32 sites I' per unit cell. On a purely statistical basis, in approaching 8 Cu/UC the system is going from a Cu in every other sodalite unit to one Cu per sodalite (see Fig. 1). At 8 Cu/UC about 6% of Cu pairs lie very close to one another at opposite ends of a hexagonal prism, around 19% lie approximately one sodalite diameter of ~ 0.7 nm apart, and the other approximately 75% lie nearer to two sodalite diameters or 1.4 nm apart. However, on average every Cu^{2+} added after 8 Cu/UC must lie less than 0.7 nm apart from another Cu^{2+} in the same sodalite unit. Thus as the value of 8 Cu/UC is traversed, this detailed Cu siting analysis shows the effective Cu–Cu distance going from greater than 1.2 nm to markedly less than 1.2 nm in agreement with the marked relaxation and EPR averaging transitions at these degrees of Cu exchange in Fig. 6.

6. Summary

In this work the exchange of Cu^{2+} into X Faujasite zeolite is shown by EPR spectral and pulsed EPR relaxation measurements to begin into site I', where it lies coordinated to a hexagonal prism face with Si:Al ratios of predominantly 4:2 and 5:1. Spin–spin interactions influence EPR g -value averaging, spin–spin relaxation, and spin spectral diffusion in a highly Cu exchange dependent manner. Spin–lattice relaxation is relatively independent of the degree of Cu exchange. The marked increase observed in spin–spin relaxation and g -value averaging at 8 Cu/UC and an effective Cu–Cu distance of 1.2 nm can be understood in terms of filling sodalite cages with an average of 1 Cu^{2+} each.

Acknowledgements

The authors are grateful for the support of the SAIC Corporation, the Institute for Hazardous Materials Management, and the Binghamton University College of Arts and Sciences for their support. We thank the referees for several helpful comments.

Appendix A. Supplementary data

Supplementary data associated with this article can be found, in the online version, at [doi:10.1016/j.chemphys.2006.09.011](https://doi.org/10.1016/j.chemphys.2006.09.011).

References

- [1] V.Y. Borovkov, M. Jiang, Y. Fu, J. Phys. Chem. B. 103 (1999) 5010.
- [2] G.T. Palomino, P. Fiscaro, S. Bordiga, A. Zecchina, E. Giamello, C. Lamberti, J. Phys. Chem. B. 104 (2000) 4064.

- [3] H.S. Lee, K. Seff, *J. Phys. Chem.* 85 (1981) 397.
- [4] S. Deshpande, D. Srinivas, P. Ratnasamy, *J. Catal.* 188 (1999) 261.
- [5] B.M. Weckhuysen, A.A. Verberckmoes, L. Fu, R.A. Schoonheydt, *J. Phys. Chem.* 100 (1996) 9456.
- [6] L. Trouillet, T. Toupance, F. Villain, C. Louis, *Phys. Chem. Chem. Phys.* 2 (2000) 2005.
- [7] F.X.L. Xamena, P. Fiescaro, G. Berlier, A. Zecchina, G.T. Palomino, C. Prestipino, S. Bordiga, E. Giamello, C. Lamberti, *J. Phys. Chem. B.* 107 (2003) 7036.
- [8] M. Anpo, M. Matsuoka, Y. Shioya, H. Yamashita, E. Giamello, C. Morterra, M. Che, H.H. Patterson, S. Webber, S. Ouellette, M.A. Fox, *J. Phys. Chem.* 98 (1994) 5744.
- [9] S. Kieger, G. Delahay, B. Coq, B. Neveu, *J. Catal.* 183 (1999) 267.
- [10] S. Uppili, K.J. Thomas, E.M. Crompton, V. Ramamurthy, *Langmuir* 16 (2000) 265.
- [11] K.H. Lim, C.P. Grey, *J. Am. Chem. Soc.* 122 (2000) 9768.
- [12] I.E. Maxwell, J.J. De Boer, *J. Phys. Chem.* 79 (1975) 1874.
- [13] W. Böhlmann, A. Pöppel, D. Michel, *Coll Surf A: Physicochem Eng Asp* 158 (1999) 235.
- [14] K. Pierloot, A. Delabie, M.H. Grootaert, R.A. Schoonheydt, *Phys. Chem. Chem. Phys.* 3 (2001) 2174.
- [15] G.L. Marra, A.N. Fitch, A. Zecchina, G. Ricchiardi, M. Salvalaggio, S. Bordiga, C. Lamberti, *J. Phys. Chem. B.* 101 (1997) 10653.
- [16] A. Delabie, K. Pierloot, M. Grootaert, B.M. Weckhuysen, R.A. Schoonheydt, *Microporous Mesoporous Mater.* 37 (2000) 209.
- [17] T. Ichikawa, L. Kevan, *J. Phys. Chem.* 87 (1983) 4433.
- [18] L. Frunza, H. Kosslick, S. Frunza, A. Schonhals, *J. Phys. Chem. B.* 106 (2002) 9191.
- [19] D. Berthomieu, J. Ducere, A. Goursot, *J. Phys. Chem. B.* 106 (2002) 7483.
- [20] G.T. Palomino, S. Bordiga, A. Zecchina, *J. Phys. Chem. B.* 104 (2000) 8641.
- [21] K. Matar, D. Goldfarb, *J. Phys. Chem.* 96 (1992) 3100.
- [22] S.B. Liu, T.S. Lin, T.C. Yang, T.H. Chen, E.C. Hong, R. Ryoo, *J. Phys. Chem.* 99 (1995) 8277.
- [23] J. Dedecek, Z. Sobalik, Z. Tvaruzkova, D. Kaucky, B. Wichterlova, *J. Phys. Chem.* 99 (1995) 16327.
- [24] J. Yu, J. Kim, L. Kevan, *Microporous Mesoporous Mater* 40 (2000) 135.
- [25] P. Carl, S. Larsen, *J. Catal.* 182 (1999) 208.
- [26] P. Carl, S. Baccam, S. Larsen, *J. Phys. Chem. B.* 104 (2000) 8848.
- [27] A. Abragam, B. Bleaney, *Electron Paramagnetic Resonance of Transition Ions*, Dover, New York, 1986, p. 451.
- [28] J.C. Conesa, J. Soria, *J. Phys. Chem.* 82 (1978) 157.
- [29] T.H. Bennur, D. Srinivas, P. Ratnasamy, *Microporous Mesoporous Mater* 48 (2001) 111.
- [30] M. Iwamoto, M. Nakamura, H. Nagano, S. Kagawa, T. Seiyama, *J. Phys. Chem.* 86 (1982) 153.
- [31] R.S. Drago, *Physical Methods for Chemists*, second ed., Saunders, New York, 1992, p. 559.
- [32] D. Nachtigallova, P. Nachtigall, J. Sauer, *Phys. Chem. Chem. Phys.* 3 (2001) 1552.
- [33] W.B. Mims, *Electron Spin Echoes*, in: S. Geschwind (Ed.), *Electron Paramagnetic Resonance*, Plenum Press, New York, 1972.
- [34] K.M. Salikhov, S.A. Dzuba, A.M. Raitsimring, *J. Magn. Reson.* 42 (1981) 255.
- [35] R. Boscaino, F.M. Gelardi, *Phys. Rev. B.* 46 (1992) 14550.
- [36] J.R. Klauder, P.W. Anderson, *Phys. Rev.* 125 (1962) 912.
- [37] K.M. Salikhov, Y.D. Tsvetkov, "Electron spin-echo studies of spin-spin interactions in solids", in: L. Kevan, R. Schwartz (Eds.), *Time Domain Electron Spin Resonance*, Wiley-Interscience, New York, 1979, p. 231.
- [38] D.C. Doetschman, G.D. Thomas, *Chem. Phys.* 228 (1998) 103.
- [39] A. Schweiger, G. Jeschke, *Principles of Pulse Electron Paramagnetic Resonance*, Oxford University Press, Oxford, 2001, p. 216.
- [40] R.F. Lobo, *Introduction to the Structural Chemistry of Zeolites*, in: S.M. Auerbach, K.A. Carrado, P.K. Dutta (Eds.), *Handbook of Zeolite Science and Technology*, Marcel Dekker, New York, 2003, p. 65.
- [41] R.M. Barrer, *Zeolites and Clay Minerals as Sorbents and Molecular Sieves*, Academic Press, New York, 1978, p. 78.
- [42] P. Gallezot, Y. Ben Taarit, B. Imelik, *J. Catal.* 26 (1972) 295.
- [43] A. Abragam, B. Bleaney, *Electron Paramagnetic Resonance of Transition Ions*, Dover, New York, 1986, p. 541.
- [44] R. Owenius, M. Engstrom, M. Lindgren, M. Huber, *J. Phys. Chem. A.* 105 (2001) 10967.
- [45] S. Patchkovskii, T. Ziegler, *J. Am. Chem. Soc.* 122 (2000) 3506.
- [46] P.J. Carl, S.C. Larsen, *J. Phys. Chem. B* 104 (2000) 6568.